11686-2001

DL/SCI/TM20A

technical memorandum Daresbury Laboratory

DL/SCI/TM20A

SOME CONSIDERATIONS OF FEEDBACK LOOP DESIGN FOR THE SRS STORAGE RING R.F. SYSTEM

by

D. J. BELL, P. A. COOK and N. MUNRO, University of Manchester Institute of Science and Technology (UMIST);

and

T. E. SWAIN, Daresbury Laboratory.

MARCH 1980

LENDING Copy

Science Research Council

Daresbury Laboratory

© SCIENCE RESEARCH COUNCIL 1980

Enquiries about copyright and reproduction should be addressed to:—
The Librarian, Daresbury Laboratory, Daresbury, Warrington, WA4 4AD.

IMPORTANT

The SRC does not accept any responsibility for loss or damage arising from the use of information contained in any of its reports or in any communication about its tests or investigations.

CONTENTS

1. INTRODUCTION

Early SRS notes[1] presented r.f. system operating conditions for the storage ring, and a subsequent Technical Memorandum[2] considered this further and dealt with some general aspects of feedback loop design. In this latter report it was demonstrated that, although the operating conditions would always ensure open-loop stability, an intensity-dependent coupling between feedback loops could possibly promote instability at below the intended beam current unless special design precautions were taken. Problems of this nature had also been encountered on the CERN PS Booster under conditions of severe beam loading[3].

Subsequent work at the UMIST Control Systems Centre has considered specific aspects of loop design and arrived at a number of options.

This report is confined to presentation of the results of this exercise. Derivations and background are available in the literature[4] and in particular will be presented in a forthcoming report.

2. MATHEMATICAL SYSTEM MODELS

The interaction between a bunched beam and the r.f. system may be described in a number of ways. If we can formulate an expression for the effective longitudinal impedance of the system as seen by the beam, as a function of frequency, then the use of standard stability theory[5] leads directly to calculation of the time dependence of the motion, which must be adequately damped for stable operation. While this "impedance" will contain any feedback loop parameters, and thus, in principle permit evaluation of loop design, in practice it is more convenient to adopt an alternative formulation in terms of system variables to allow the use of standard control system theory.

Analysis then yields a set of coupled, non-linear differential equations in these variables. This set comprises

(a) the usual "synchrotron equations" relating the beam phase and energy deviation to the cavity voltage, which is in general amplitude and phase modulated.

(b) equations relating this amplitude and phase modulation to both the beam induced voltage resulting from its phase motion and any generator drive modulation resulting from closed feedback loops.

(c) for closed loop operation, loop equations relating this generator drive modulation to detected error quantities such as, in the SRS, the cavity voltage and phase devlation.

In this form the equations are rather intractable, and the technique adopted is to linearise about a stationary state, i.e. a possible operating condition, and use standard techniques for evaluating the natural frequencies of the resultant set of coupled linear differential equations. Note that by this linearisation, any information about separatrices has been lost, and thus the formulation is only valid for small deviations about a stationary state.

This system has a matrix representation, and for consideration of feedback may be considered in two components:

(1) A matrix equation relating small changes in the cavity voltage amplitude and phase to small changes in the generator drive input amplitude and phase[6].

$$\begin{pmatrix} \Delta V \\ V\Delta\phi_v \end{pmatrix} = \frac{N(s)}{d(s)} \begin{pmatrix} \Delta V_g \\ V_g\Delta\phi_g \end{pmatrix} \qquad (1)$$

$\frac{N(s)}{d(s)}$ is the beam cavity open loop transfer function matrix.

N(s) is a matrix of polynomials in the derivative d/dt, which, after Laplace transform, yields a matrix of polynomials in S, over a common denominator polynomial d(s), the coefficients of which relate to the operating conditions of the beam-cavity system.

(2) The feedback matrix equation relating small changes in the generator output to the observed changes in the cavity voltage.

$$\begin{pmatrix} \Delta V_g \\ V_g \Delta\phi_g \end{pmatrix} = F \begin{pmatrix} \Delta V \\ V\Delta\phi_v \end{pmatrix} \qquad (2)$$

In general F may be a product of matrices, and will in principle contain feedback characteristics such as bandwidth, gain and delay. This then yields the closed loop transfer function matrix for the system.

$$\left(I + \frac{FN(s)}{d(s)}\right)^{-1} \frac{N(s)}{d(s)} = \frac{\text{Adj}\left(I + \frac{N(s)}{d(s)}\right) G}{\left|I + \frac{N(s)}{d(s)}\right|}$$

Two types of feedback may be distinguished here. If F is a simple diagonal matrix $\begin{pmatrix} f_{11} & 0 \\ 0 & f_{22} \end{pmatrix}$ then amplitude feedback is only derived from amplitude error, and similarly for phase, and the feedback is described as single loop. If F has non-zero off-diagonal elements, the feedback is described as multivariable.

Since the beam-cavity matrix has non-zero off-diagonal elements, deriving in part from the beam loading, the system is described as having interaction, and the analysis of such a closed loop situation poses special problems.

The standard single loop evaluation techniques of Bode and Nyquist were originally devised for non-interacting systems, and can only be applied - in a modified form - to interacting systems under certain conditions which were shown[2] to be violated for the storage ring operating parameters.

The potentially worst condition from a control point of view is that of full accumulated beam at injection energy, where the beam loading is relatively most severe, and effort was concentrated on this situation. As this condition is approached during stacking, the cavity tuner has to make its most rapid movements to compensate for changing reactive beam loading, and the stability margin, in terms of detune, shrinks. (At 1.0 A

the required detune is ~ 400 KHz and the "Robinson" unstable detune region extends from a few KHz to ~ 396 KHz.) In order to ensure that an adequate detune is provided a deliberate offset may be required leading to a reactive mismatch characterised by a non-zero angle ϕ_g between the generator drive current and cavity volts. Accordingly the system has been examined with some estimated values of likely ϕ_g, together with the situation at high energy which was expected to be more readily controlled.

The following cases were considered:

(A) Accumulation with $I_b = 1.0$ A, $\phi_g = 0^\circ$, and $V_{ep} = 0.6$ Mv

(B) Accumulation with $I_b = 1.0$ A, $\phi_g = 5.6^\circ$, and $V_{ep} = 0.6$ Mv

(C) Accumulation with $I_b = 1.0$ A, $\phi_g = 12^\circ$, and $V_{ep} = 0.6$ Mv

(D) Storage with $I_b = 1.0$ A, $\phi_g = 0^\circ$, and $V_{ep} = 1.6$ Mv

(E) Storage with $I_b = 1.0$ A, $\phi_g = 0^\circ$, and Vep = 1.9 Mv

The various transfer-function matrix models for each of the above cases are detailed in table 1 in the form of a set of numerator polynomials $n_{ij}(s)$; i,j = 1,2; over a common denominator polynomial d(s); where these polynomials have the form

$$n_{ij}(s) = \alpha_3 s^3 + \alpha_2 s^2 + \alpha_1 s^1 + \alpha_0 s^0 \qquad (3)$$

$$d(s) = s^4 + d_3 s^3 + d_2 s^2 + d_1 s^1 + d_0 s^0 \qquad (4)$$

again with coefficients that depend on the operating condition.

The coefficients of the polynomials defining the various models are very large and might pose severe numerical problems for the analysis and simulation procedures to be used. It was therefore decided to apply some frequency scaling (i.e. substitute $\tilde{s} = 10^{-6}s$), normalisation (i.e. divide every coefficient by 10^{24}, and some amplitude scaling (i.e. multiply every numerator coefficient by 10^6). This resulted in a set of scaled models as shown in Table 2. In these models, the frequency characteristics must be interpreted in M-Hertz (or M-radians per second), and the outputs from these models, namely cavity-voltage amplitude and phase must be

interpreted in μ-volts and μ-radians. Upper case letters will be used to refer to the various scaled models, described in table 2.

Some care was required in generating these coefficients, as a small difference between two large numbers could be significant.

3. CONTROL STUDIES

The initial report[2] had demonstrated that the beam cavity system showed a beam intensity dependent "interaction" resulting from the off diagonal elements of the system matrix becoming increasingly significant as beam loading and cavity detuning increased. A particular design technique developed at UMIST hinges on the removal of this interaction by suitable analytic operations on the matrix - described as compensation - which must have, however, for subsequent practical purposes, a convenient physical realisation in terms of circuitry. A matrix of constants may be readily diagonalised by a variety of methods; for a matrix of polynomials however this is more difficult, and, it has been shown[7] that only a partial diagonalisation is required, with the significance of the off diagonal elements being reduced to a suitable level rather than completely removed. This state is referred to as "diagonal dominance" in the control system literature.

Accordingly work commenced on the design of a possible compensator for the system using the inverse Nyquist Array method.

3.1 Inverse Nyquist Array method

The inverse Nyquist array (INA) of the system transfer matrix is generated by the following prescription

$$\hat{G}(j\omega) = G^{-1}(\tilde{s}) \text{ evaluated at } \tilde{s} = j\omega$$

$$G^{-1}(\tilde{s}) = \frac{\text{Adj}(G)}{\det G} = \frac{\begin{pmatrix} g_{22} & -g_{12} \\ -g_{21} & g_{11} \end{pmatrix}}{|G|} = \begin{pmatrix} \hat{g}_{11} & \hat{g}_{12} \\ \hat{g}_{21} & \hat{g}_{22} \end{pmatrix}$$

This is evaluated as a function of ω over the range $0 \leq \omega < 0.5$ rad/s

(scaled). In particular we are concerned with whether the off-diagonal elements, $\hat{g}_{12}$, and $\hat{g}_{21}$, are greater than $\hat{g}_{11}$ and $\hat{g}_{22}$ respectively. This comparison is effected by drawing circles, (Gershgorin circles) centre, $\hat{g}_{11}$ and $\hat{g}_{22}$, of radii $\hat{g}_{12}$ and $\hat{g}_{21}$ respectively. If these circles enclose the origin the system is non-dominant. Numerous examples appear in reference 2 and one also in fig. 1 of this report for the open loop situation at injection energy with full accumulated beam. An examination of these diagrams reveals the following features. Elements $\hat{g}_{11}(j\omega)$ and $\hat{g}_{21}(j\omega)$ were very similar in nature, as might be expected from their transfer function representation. Element $\hat{g}_{12}(j\omega)$ was second order and tended to increase rapidly in modulus with increasing frequency. However, element $\hat{g}_{21}(j\omega)$ appeared to be stationary and relatively large. An explicit evaluation of $\hat{G}(s)$ was therefore carried out for case (A) of Table 2 to determine the exact nature of the inverse elements, and yielded the following matrix

$$G^{-1}(s) = \hat{G}(s) = \frac{\begin{pmatrix} \tilde{s}^3 + .107\tilde{s}^2 + 1.39\tilde{s} + 1.37 & -2.54\tilde{s}^2 - 3.546 \\ 2.544\tilde{s}^2 + .019 & \tilde{s}^3 + .107\tilde{s}^2 + 1.39\tilde{s} + .162 \end{pmatrix}}{2.544s^2 + .019}$$

$$= \frac{N(s)}{d(s)}$$

Note that $n_{21}(s)$ and $d(s)$ cancel removing the frequency dependence of $\hat{g}_{21}(s)$, and also that the poles of $\hat{G}(s)$ which are the zeros of $\det G(s)$, (i.e. $d(s)$) are at $s = \pm j\,1.181$, which corresponds to the angular incoherent synchrotron frequency of 187 KHz. This frequency however is not in general a natural frequency of the coupled system. As we approach the synchrotron angular frequency, elements $\hat{g}_{11}$, $\hat{g}_{22}$, and $\hat{g}_{12}$ become indefinitely large, as shown by the rapidly enlarging circles on fig. 1. A detailed investigation was carried out to develop a suitable compensator using row operations on the transfer matrix. This readily succeeded in removing the interaction from $\hat{g}_{12}$, sufficiently to obtain diagonal dominance, except in the vicinity of ω_s. However the encirclement associated with $\hat{g}_{21}$ was not readily removed. Figure 2 demonstrates this for case A with simple row operations on the matrix indicated.

Because of the nature of the system, it appears difficult to achieve diagonal dominance in a simple way. In view of this the technique appears to be inappropriate for the problem, and was therefore not pursued further.

3.2 Design using the multivariable root-locus

The multivariable root-locus method, as used in this study, is simply a means of assessing the performance of a control scheme by plotting the positions of the closed-loop system poles, i.e. natural frequencies as an overall gain parameter is varied. Suppose the general configuration is as follows:

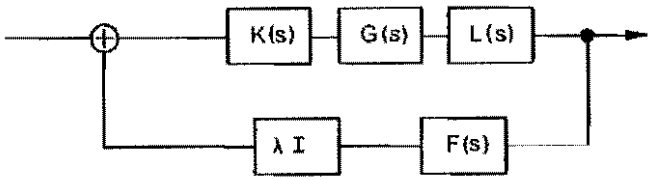

The introduction of the adjustable gain λI, where I is the unit matrix and λ is a scalar parameter, is equivalent to simply multiplying one of the transfer function matrices in the loop by λ. (It does not matter which one, since λ could equally well have been put in any other part of the loop, so far as the root-loci are concerned.) As λ is varied, the poles of the closed-loop system will move about in the complex s-plane. For a given value of λ, the positions of these moving poles are the roots of the equation

$$\det [I + \lambda F(s)L(s)G(s)K(s)] = 0 .$$

For the open loop situation this reduces to a quartic equation with, in general, conjugate pairs of roots. For feedback with dynamics such as integration, a higher degree equation with additional roots results, which latter must however coalesce with the open loop roots, as $\lambda \to 0$. (See reference 2 for an alternative presentation of the open-loop roots, as a function of operating parameters.)

In the multivariable root-locus method, these roots are plotted on the complex plane, as λ is varied over a range of values. Preferably, the system should remain stable (all roots in the left half-plane) for all positive λ. In any case, it should be stable for the nominal value of λ intended to be used in the actual design, and for a wide range of variation about this value. Otherwise, the stability will be sensitive to variations in parameter values, which is clearly undesirable. In particular, the system should remain stable for all λ between 0 and the nominal value, since otherwise instabilities will arise if the effective gain is reduced, e.g. due to either saturation effects, or the loop being opened. The root-loci will also indicate suitable magnitude to be chosen for λ in order to achieve, for example, maximum damping. Clearly, this method gives more information than would be obtained from simply calculating the closed-loop poles for a fixed gain. Still more information would be given by putting different variable gains in different loops, and thus exploring stability in a "gain space". This can also be done by multivariable root-locus methods, and may be appropriate for a more detailed investigation.

In the present study, we have set $F(s) = L(s) = I$ (the unit matrix), and plotted in figs. 3-5 the root-loci for various choices of precompensator K(s) and for several different G(s) corresponding to different operating conditions (cases A,C,D,E). The simplest scheme investigated consisted of equal constant gains (i.e. proportional action) in both loops, so that

$$K(s) = I = \begin{pmatrix} 1 & 0 \\ 0 & 1 \end{pmatrix}$$

It was found that stability was maintained for all positive values of λ in all cases, so that, from this point of view, the design was already satisfactory. (Some trials were also made to see the effect of putting different gains in the loops, and again the system remained stable for the cases examined, although only a rather limited investigation has been made so far.) In order to eliminate steady-state error, however, the possibility of incorporating integral action was investigated. This

also had the effect of reducing interaction, especially when placed in the second loop (generator phase to cavity-voltage phase). Accordingly, the root-loci were plotted for the choice

$$K(s) = \begin{pmatrix} 1 & 0 \\ 0 & 1 + \frac{0.1}{s} \end{pmatrix}$$

i.e. proportional action in loop 1 and proportional + integral in loop 2. Stability was still maintained in the cases examined, although with reduced damping, as expected. In particular, there was a tendancy for damping to be poor at small gain values. This became even more marked when porportional + integral action was put in each loop, with

$$K(s) = (1 + \frac{0.1}{s})\ I$$

to the extent that one case (C) became very nearly unstable for a certain range of gains. This effect is, however, considerably dependent on the choice of integral action constant and there is no particular reason to insist on 0.1. (Some other trials, on case A, indicated that 0.2 led to instability for certain gain values, while 0.05 in each loop had about the same effect as 0.1 in loop 2 only.) In any case, it seems unnecessary to have integral action in loop 1, in order to achieve satisfactory step-responses. In all cases, the root-loci indicated that the choice of $\lambda = 1$ (unity feedback), as taken in the time-response simulations, was of the right magnitude to make the damping about as good as could be achieved with these compensator structures. Other more complicated structures, with entries in all elements of K(s), were briefly examined, but did not appear to give any advantage.

3.3 System time responses

A convenient technique for system evaluation is to apply a small step drive S(t) to a given input, and note the response $r_i(t)$ on the i possible output channels. The response to a general drive (on the same input channel) f(t) is then implied by a superposition integral of the form

$$R(t) = \begin{matrix}\text{Initial} \\ \text{value} \\ \text{term}\end{matrix} + \int_0^t \frac{df_i(0)}{d\theta}\ r_i(t-\theta)\ d\theta,$$

and for drives on all channels, by further summation for linear systems. For an ideal system we would hope to see a pure step response on the appropriate output channel, and zero response on all other channels. In practice, we observe

(1) Significant transient response with overshoot and ringing, due to the cavity being a high Q circuit, and the strongly coupled beam being effectively undamped, at least at 600 MeV.

(2) Interaction manifests itself by the other output having significant transients as well as steady state error.

This computation was performed for the various system models already discussed by alternative techniques, and the results depicted in figs.6-18. For each system configuration, 4 figures give the amplitude, and phase responses of each channel to an amplitude and a phase step in turn.

3.3.1 Open loop time responses

An examination of these responses (figs. 6, 11 and 15)confirms that the interaction present in the beam-cavity is worst for full accumulated beam at injection energy. It also increases as the cavity detune offset is increased; this is expected as the non-zero ϕg now resolves a given step into components in phase, and in quadrature with respect to the cavity voltage. In all cases the cavity voltage phase is significantly disturbed by changes in generator drive amplitude, and is more sensitive to this input than to changes in the drive phase. Also, there is considerable breakthrough of lightly damped high frequency oscillation superposed in the voltage amplitude response, when the generator-drive phase is altered. The frequency of these oscillations typically varies from 445.6 KHz to 221 KHz as the system moves from injection energy (with $\phi g = 0$) to full energy with Vep = 1.9 MV.

Other notable features of the time responses of the open loop system are somewhat lower frequency (synchrotron) oscillations on both

outputs which are gradually damped out as the system moves from the accumulation phase to the storage phase; the frequency of these oscillations varying from 91 krad/s at accumulation (with generator phase angle $\phi g = 0^{\circ}$) to 29 krad/s at full energy (with Vep = 1.9 MV). Also, as the beam-cavity system progresses through ramping to storage mode, the steady-state gains of the various transmission paths change. The most significant of these variations occurs in the path from generator drive amplitude to cavity-voltage amplitude and in the path from generator drive phase to cavity-voltage amplitude; the latter variation being helpful in control terms. However, the former variation may require scheduling of the gain in the feedback loop from cavity-voltage amplitude to generator drive amplitude to avoid reduction of stability margins during ramping.

The variations in the poles of the scaled open-loop systems for each case studied, are shown in table 3, and the corresponding steady-state gain values for each case are shown in table 4.

3.3.2 Closed loop responses

These were obtained for a number of the feedback options discussed in section 3.2, using a gain parameter appropriate to unity feedback, which appeared to maximise damping rates as given by the root-locus plots. The conclusions of section 3.2 are supported, proportional feedback in both loops gives a substantial suppression of overshoot and ringing, as well as interaction, while integral action eliminates the steady state error in the interacting output, at the expense of increased transients.

4. CONCLUSIONS

The immediate conclusion is that a simple proportional feedback in both loops will be of considerable benefit in stabilising the system against disturbance. The use of loop dynamics, i.e. integration, will reduce steady state error, but at the expense of reduced damping, and, indeed, even approaching instability at low loop gain. To minimise this undesirable effect the integral action should be confined to the phase loop, and a proportional factor of about unity adopted. The result concerning the advantages of proportional feedback seems in agreement with earlier SPEAR work[4]. Much emphasis had been placed on examining the error conditions of excess detune, (D and C). One interpretation of the

effect of proportional feedback is that the unstable detune region predicted by the Robinson criterion is reduced in width, and thus, the use of an excessive detune offset may be avoided, giving a more satisfactory matched system. This reduction of the unstable region by feedback remains to be evaluated for the whole operating region, and, ideally, a physical interpretation of this behaviour provided.

Also, in principle, feedback could be utilised to enable higher efficiency operation of the r.f. system. At 2 GeV in the SRS, the high over-voltage defines the cavity power for given impedance, with 1.0 A beam present the efficiency (when matched) is

$$n = \frac{Pb}{Pb + Pc} = 0.66 .$$ At lower energies the opportunity will be available to lower the cavity voltage to such level as to increase n while still maintaining lifetime. In a future r.f. design this could enable a higher impedance structure to be used to reduce structure dissipation relative to beam power, subject to matching and detuning limitations.

Some areas remain for further study:-

(a) Analysis of a multi-cavity system, with non-ideal isolation between the cavities and the Klystron, and bandwidth limitation of feedback loops.

(b) Effect of Q_s splitting on the beam cavity interaction. One interpretation of Q_s splitting is in terms of coupling of the normal modes of oscillation of the bunched beam. With the Q_s cavity driven at 750 MHz, the time constants of the accelerating cavity interaction will now be influenced by the Q_s cavity parameters.

(c) Effect of the use of a cavity powered at a higher harmonic of the r.f.

REFERENCES

1. SRS Notes 73/10, 74/49, 74/60 and 74/62.

2. D. J. Bell, N. Munro and T. E. Swain, DL/SRF/TM5(1970).

3. F. Pedersen, IEEE Trans. NS-23 (1975) 1906.

4. M. Lee, Spear Report 31 (1970); Spear Report 30 (Revised) (1973); K. W. Robinson, CEA Report 11 (1956); CEAL Report 1010 (1964).

5. F. J. Sacherer, CERN Report CERN/PS/BR/77-5 (1977).

6. M. Donald, MD/MN/03, also BL/TH/37. Early Daresbury Reports.

7. H. H. Rosenbrock, Computer Aided Control System Design. Academic Press, 1974.

TABLE 1.

Numerator and denominator polynomials (unscaled) for the five cases

Case	Element	s^4	s^3	s^2	s^1	s^0
(a)	$\eta_{11}(s)$	-	1.0	1.07360×10^5	1.39410×10^{12}	1.62480×10
	$\eta_{12}(s)$	-	-	2.54416×10^6	-	1.93183×10
	$\eta_{21}(s)$	-	-	-2.54416×10^6	-	-3.54677×10
	$\eta_{22}(s)$	-	1.0	1.07360×10^5	1.39410×10^{12}	1.36862×10
	$d(s)$	1.0	2.14720×10^5	7.87839×10^{12}	2.99341×10^{17}	6.75183×10
(b)	$\eta_{11}(s)$	-	9.9522741×10^{-1}	3.5394113×10^5	1.3874465×10^{12}	1.6195371×10^{17}
	$\eta_{12}(s)$	-	$-9.7582847 \times 10^{-2}$	2.5095795×10^6	$-1.3604025 \times 10^{11}$	$-1.3309763 \times 10^{16}$
	$\eta_{21}(s)$	-	9.7582847×10^{-2}	-2.5095795×10^6	1.3604025×10^{11}	-3.4998085×10
	$\eta_{22}(s)$	-	9.9522741×10^{-1}	3.5394113×10^5	1.3874465×10^{12}	4.8067693×10^{17}
	$d(s)$	1.0	2.14720×10^5	7.8173638×10^{12}	2.9934115×10^{17}	2.3666348×10^{22}
(c)	$\eta_{11}(s)$	-	9.7814761×10^{-1}	6.3397512×10^5	1.3636356×10^{12}	1.6294551×10^{17}
	$\eta_{12}(s)$	-	$-2.0791164 \times 10^{-1}$	2.4662460×10^6	$-2.8984961 \times 10^{11}$	$-1.4885241 \times 10^{16}$
	$\eta_{21}(s)$	-	2.079116×10^{-1}	-2.4662460×10^6	2.8984961×10^{11}	$-3.4408112 \times 10^{18}$
	$\eta_{22}(s)$	-	9.7814761×10^{-1}	6.3397512×10^5	1.3636356×10^{12}	8.7128596×10^{17}
	$d(s)$	1.0	2.14720×10^5	7.878394×10^{12}	2.9934115×10^{17}	6.7518286×10^{22}
(d)	$\eta_{11}(s)$	-	1.0	1.77150×10^5	1.39410×10^{12}	3.5707481×10
	$\eta_{12}(s)$	-	-	8.5247014×10^5	-	6.2862351×10
	$\eta_{21}(s)$	-	-	-8.5247014×10^5	-	$-1.1782226 \times 10^{18}$
	$\eta_{22}(s)$	-	1.0	1.77150×10^5	1.39410×10^{12}	1.3685681×10
	$d(s)$	1.0	3.5430×10^5	2.1521874×10^{12}	4.9492963×10^{17}	3.5590716×10^{22}
(e)	$\eta_{11}(s)$	-	1.0	1.98450×10^5	1.39410×10^{12}	4.1645914×10
	$\eta_{12}(s)$	-	-	7.4557587×10^5	-	-9.2681314×10
	$\eta_{21}(s)$	-	-	-7.4557587×10^5	-	-1.0206063×10
	$\eta_{22}(s)$	-	1.0	1.98450×10^5	1.39410×10^{12}	1.3685914×10
	$d(s)$	1.0	3.9690×10^5	1.9893658×10^{12}	5.5331829×10^{17}	4.0856724×10^{22}

TABLE 2.

Numerator and denominator polynomials (scaled) for the five cases

Case	Element	$\tilde{s}^4$	$\tilde{s}^3$	$\tilde{s}^2$	$\tilde{s}^1$	$\tilde{s}^0$
(A)	$\eta_{11}(\tilde{s})$	-	1.0	1.07360×10^{-1}	1.39410×10^{0}	1.62480×10^{-1}
	$\eta_{12}(\tilde{s})$	-	-	2.54416×10^{0}	-	1.93183×10^{-2}
	$\eta_{21}(\tilde{s})$	-	-	-2.54416×10^{0}	-	-3.54677×10^{0}
	$\eta_{22}(\tilde{s})$	-	1.0	1.07360×10^{-1}	1.39410×10^{0}	1.36862×10^{-1}
	$d(\tilde{s})$	1.0	2.14720×10^{-1}	7.87839×10^{0}	2.99341×10^{-1}	6.75183×10^{-2}
(B)	$\eta_{11}(\tilde{s})$	-	9.9522741×10^{-1}	3.5394113×10^{-1}	1.3874465×10^{0}	1.6195371×10^{-1}
	$\eta_{12}(\tilde{s})$	-	$-9.7582847 \times 10^{-2}$	2.5095795×10^{0}	$-1.3604025 \times 10^{-1}$	$-1.3309763 \times 10^{-2}$
	$\eta_{21}(\tilde{s})$	-	9.7582847×10^{-2}	-2.5095795×10^{0}	1.3604025×10^{-1}	-3.4998085×10^{0}
	$\eta_{22}(\tilde{s})$	-	9.9522741×10^{-1}	3.5394113×10^{-1}	1.3874465×10^{0}	4.8067693×10^{-1}
	$d(\tilde{s})$	1.0	2.14720×10^{-1}	7.8173638×10^{0}	2.9934115×10^{-1}	2.3666348×10^{-2}
(C)	$\eta_{11}(\tilde{s})$	-	9.7814761×10^{-1}	6.3397512×10^{-1}	1.3636356×10^{0}	1.6294551×10^{-1}
	$\eta_{12}(\tilde{s})$	-	$-2.0791164 \times 10^{-1}$	2.4662460×10^{0}	$-2.8984961 \times 10^{-1}$	$-1.4885241 \times 10^{-2}$
	$\eta_{21}(\tilde{s})$	-	2.0791164×10^{-1}	-2.466246×10^{0}	2.8984961×10^{-1}	-3.4408112×10^{0}
	$\eta_{22}(\tilde{s})$	-	9.7814761×10^{-1}	6.3397512×10^{-1}	1.3636356×10^{0}	8.7128596×10^{-1}
	$d(\tilde{s})$	1.0	2.14720×10^{-1}	7.878394×10^{0}	2.9934115×10^{-1}	6.7518286×10^{-2}
(D)	$\eta_{11}(\tilde{s})$	-	1.0	1.77150×10^{-1}	1.39410×10^{0}	3.5707481×10^{-1}
	$\eta_{12}(\tilde{s})$	-	-	8.5247014×10^{-1}	-	6.2862351×10^{-4}
	$\eta_{21}(\tilde{s})$	-	-	$-8.5247014 \times 10^{-1}$	-	-1.1782226×10^{0}
	$\eta_{22}(\tilde{s})$	-	1.0	1.77150×10^{-1}	1.39410×10^{0}	1.3685681×10^{-1}
	$d(\tilde{s})$	1.0	3.5430×10^{-1}	2.1521875×10^{0}	4.9392963×10^{-1}	3.5590716×10^{-2}
(E)	$\eta_{11}(\tilde{s})$	-	1.0	1.98450×10^{-1}	1.39410×10^{0}	4.1645914×10^{-1}
	$\eta_{12}(\tilde{s})$	-	-	7.4557587×10^{-1}	-	$-9.2681314 \times 10^{-5}$
	$\eta_{21}(\tilde{s})$	-	-	$-7.4557587 \times 10^{-1}$	-	-1.0206063×10^{0}
	$\eta_{22}(\tilde{s})$	-	1.0	1.98450×10^{-1}	1.39410×10^{0}	1.3685914×10^{-1}
	$d(\tilde{s})$	1.0	3.9390×10^{-1}	1.9893658×10^{0}	5.5331829×10^{-1}	4.0856724×10^{-2}

TABLE 3

Poles of the scaled open-loop system for the five cases

Case	Poles
A	- 0.088 ± j 2.80, - 0.019 ± j 0.091
B	- 0.088 ± j 2.80, - 0.019 ± j 0.052
C	- 0.088 ± j 2.80, - 0.019 ± j 0.091
D	- 0.060 ± j 1.45, - 0.116 ± j 0.057
E	- 0.056 ± j 1.39, - 0.142 ± j 0.029

TABLE 4

Steady-state gain values for the five cases

Case	$g_{11}(0)$	$g_{12}(0)$	$g_{21}(0)$	$g_{22}(0)$
A	2.406	0.2861	- 52.53	2.027
B	6.843	- 0.5624	- 147.9	20.31
C	2.413	- 0.2205	- 50.96	12.90
D	10.03	0.01766	- 33.10	3.845
E	10.19	0.002268	- 24.98	3.349

FIGURE CAPTIONS

Fig. 1 Gershgorin circle diagram for case A uncompensated. Note origin encirclement over a substantial frequency range for both diagonal elements.

Fig. 2 Gershgorin diagram for case A with an attempted compensation. Note that for the upper matrix row, the resonant encirclement in the region of $\omega = \omega_g$. For the lower row the encirclement is still non-resonant.

Fig. 3 Root locus plots.

Vertical Axis — Frequency

Horizontal — Damping time constant

Arrows indicate increasing λ in range - 12 db to + 12 db

(a) Case (A) $K(s) = \begin{pmatrix} 1 & 0 \\ 0 & 1 \end{pmatrix}$

(b) Case (A) $K(s) = \begin{pmatrix} 1 & 0 \\ 0 & 1+\frac{0.1}{s} \end{pmatrix}$

(c) Case (A) $K(s) = \begin{pmatrix} 1+\frac{0.1}{s} & 0 \\ 0 & 1+\frac{0.1}{s} \end{pmatrix}$

(d), (e), (f) aa (a), (b) and (c), enlarged to show region near origin.

Fig. 4 Root locus plots.

(a) Case (C) $K(s) = \begin{pmatrix} 1 & 0 \\ 0 & 1 \end{pmatrix}$

(b) Case (C) $K(s) = \begin{pmatrix} 1 & 0 \\ 0 & 1+\frac{0.1}{s} \end{pmatrix}$

(c) Case (C) $K(s) = \begin{pmatrix} 1+\frac{0.1}{s} & 0 \\ 0 & 1+\frac{0.1}{s} \end{pmatrix}$

(d) Case (D) $K(s) = \begin{pmatrix} 1 & 0 \\ 0 & 1 \end{pmatrix}$

(e) Case (D) $K(s) = \begin{pmatrix} 1 & 0 \\ 0 & 1+\frac{0.1}{s} \end{pmatrix}$

(f) Case (D) $K(s) = \begin{pmatrix} 1+\frac{0.1}{s} & 0 \\ 0 & 1+\frac{0.1}{s} \end{pmatrix}$

Fig. 5 Root Locus Plots

(a) Case (E) $K(S) = \begin{pmatrix} 1 & 0 \\ 0 & 1 \end{pmatrix}$

(b) Case (E) $K(s) = \begin{pmatrix} 1 & 0 \\ 0 & 1+\frac{0.1}{s} \end{pmatrix}$

(c) Case (E) $K(s) = \begin{pmatrix} 1+\frac{0.1}{s} & 0 \\ 0 & 1+\frac{0.1}{s} \end{pmatrix}$

Figs. (6) - (18).

Amplitude and Phase responses to small step changes

(a) response to amplitude step

(b) response to phase step

Fig. 6 Case (A) Open loop

Fig. 7 Case (A) $K(s) = \begin{pmatrix} 1 & 0 \\ 0 & 1 \end{pmatrix}$

Fig. 8 Case (A) $K(s) = \begin{pmatrix} 1+\frac{0.1}{s} & 0 \\ 0 & 1+\frac{0.1}{s} \end{pmatrix}$

Fig. 9 Case (A) $K(s) = \begin{pmatrix} 1+\frac{0.1}{s} & 0 \\ 0 & 1 \end{pmatrix}$

Fig. 10 Case (A) $K(s) = \begin{pmatrix} 1 & 0 \\ 0 & 1 + \frac{0.1}{s} \end{pmatrix}$

Fig. 11 Case (C) Open loop

Fig. 12 Case (C) $K(s) = \begin{pmatrix} 1 & 0 \\ 0 & 1 \end{pmatrix}$

Fig. 13 Case (C) $K(s) = \begin{pmatrix} 1 + \frac{0.1}{s} & 0 \\ 0 & 1 + \frac{0.1}{s} \end{pmatrix}$

Fig. 14 Case (C) $K(s) = \begin{pmatrix} 1 & 0 \\ 0 & 1 + \frac{0.1}{s} \end{pmatrix}$

Fig. 15 Case (E) Open loop

Fig. 16 Case (E) $K(s) = \begin{pmatrix} 1 & 0 \\ 0 & 1 \end{pmatrix}$

Fig. 17 Case (E) $K(s) = \begin{pmatrix} 1 + \frac{0.1}{s} & 0 \\ 0 & 1 + \frac{0.1}{s} \end{pmatrix}$

Fig. 18 Case (E) $K(s) = \begin{pmatrix} 1 & 0 \\ 0 & 1 + \frac{0.1}{s} \end{pmatrix}$

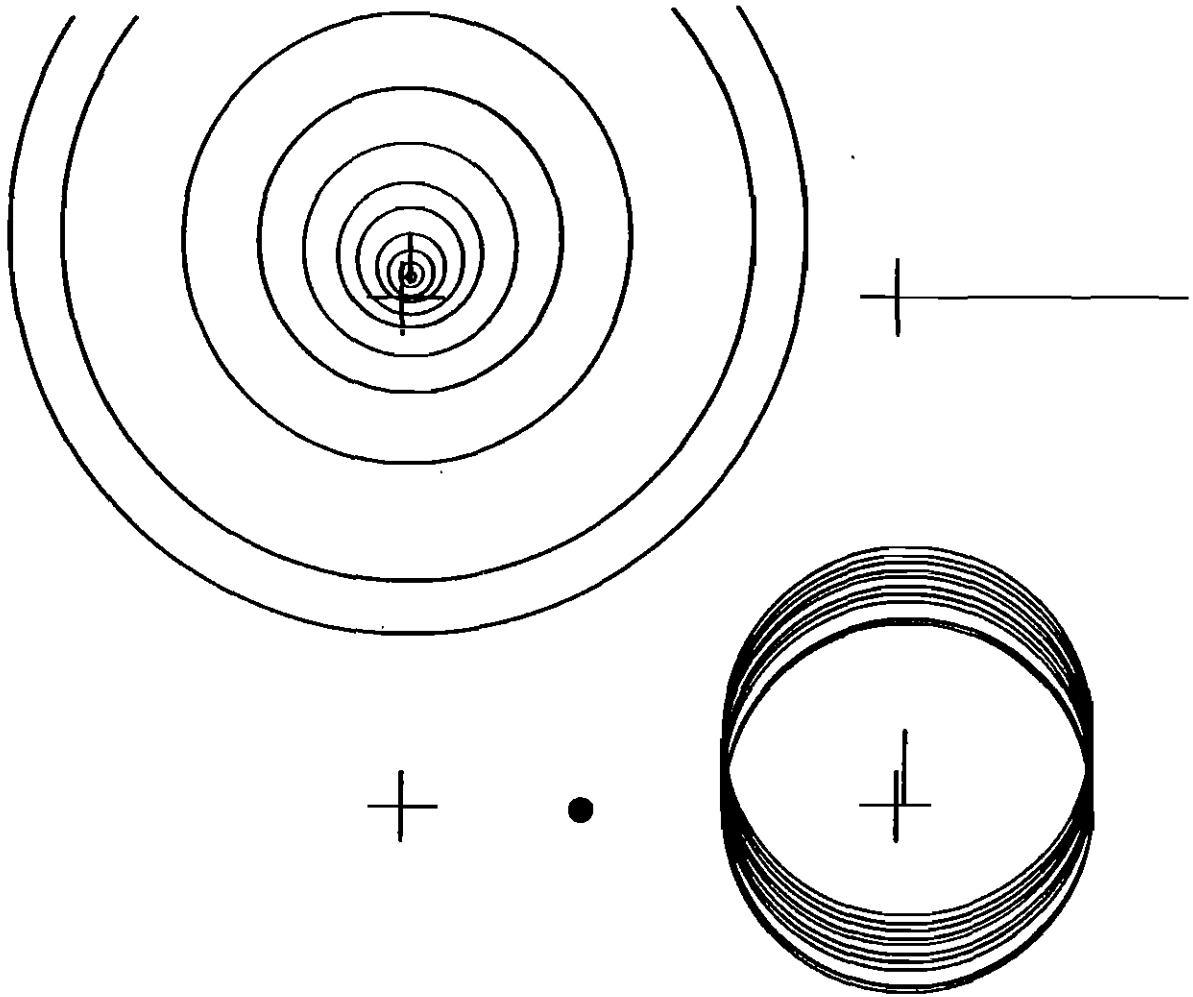

Fig. 1

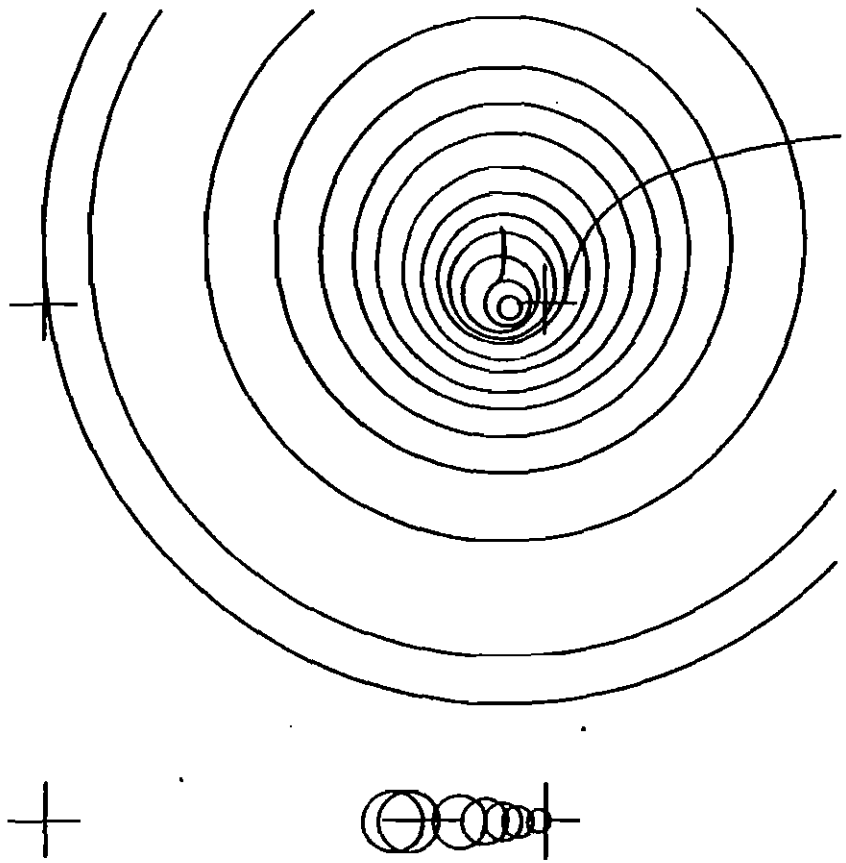

Fig.2

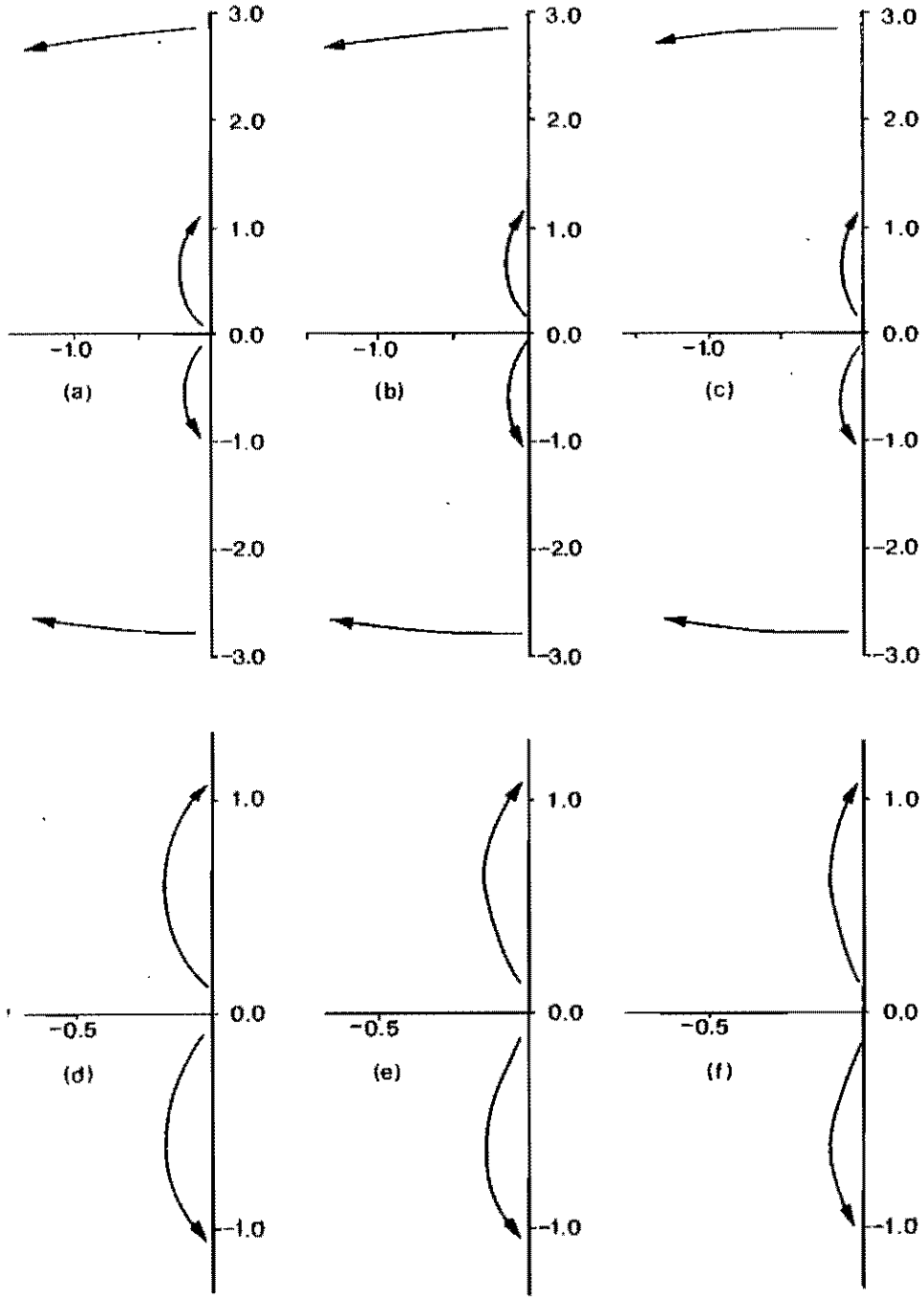

Fig. 3

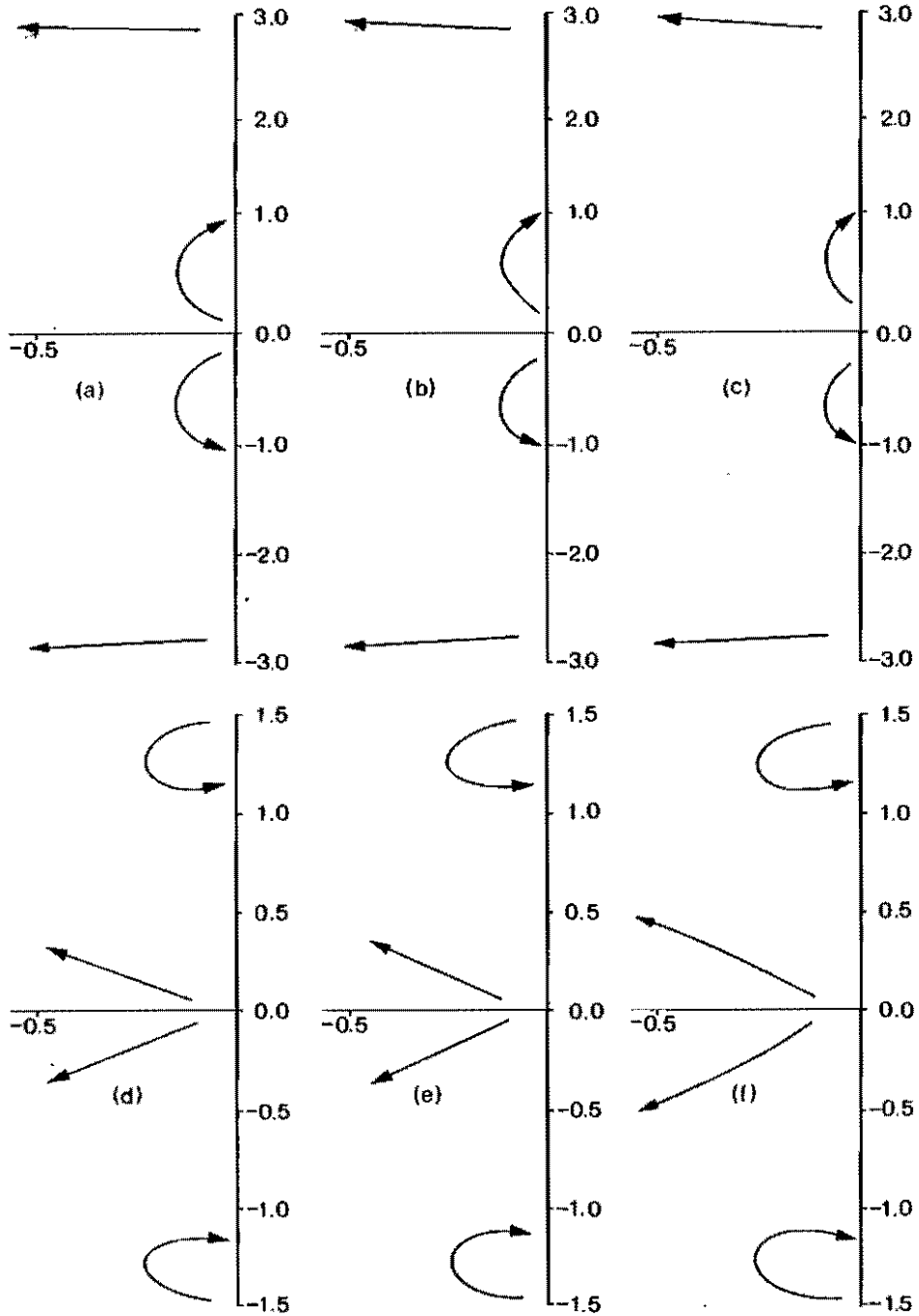

Fig.4

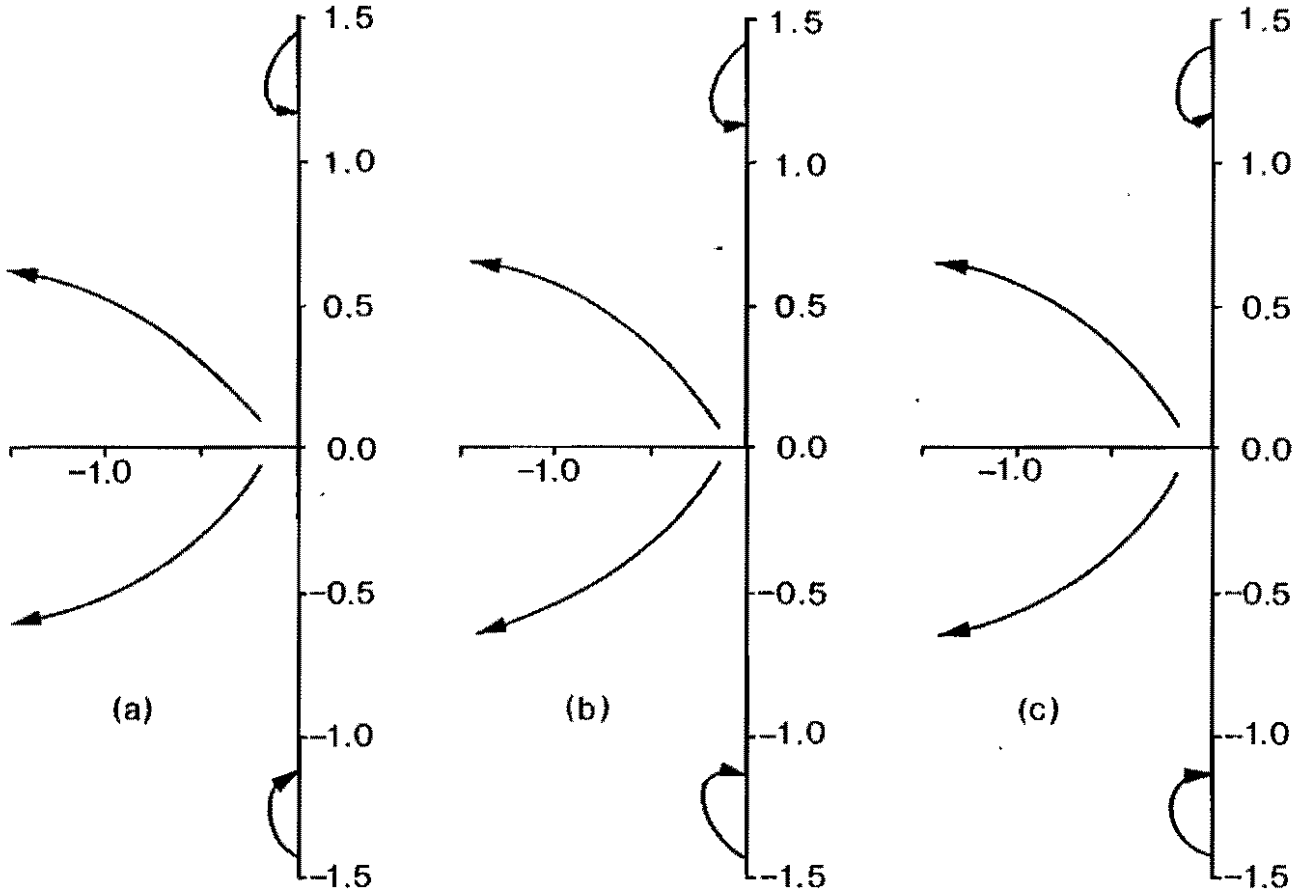

Fig.5

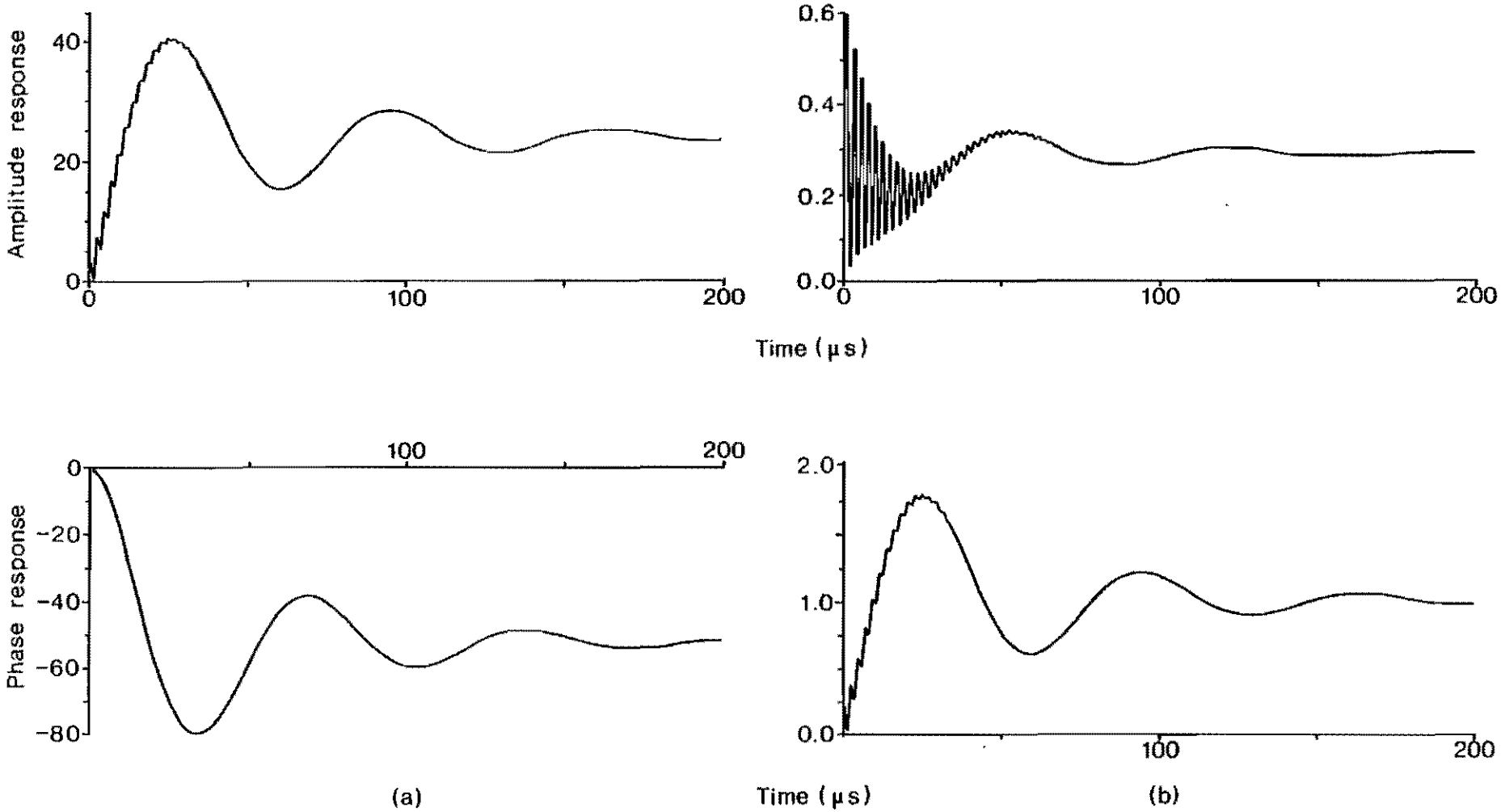
Amplitude response
40
20
0
0
100
200
0.6
0.4
0.2
0.0
0
100
200
Time (μs)
Phase response
100
200
0
-20
-40
-60
-80
2.0
1.0
0.0
100
200
Time (μs)
(a)
(b)

Fig. 6

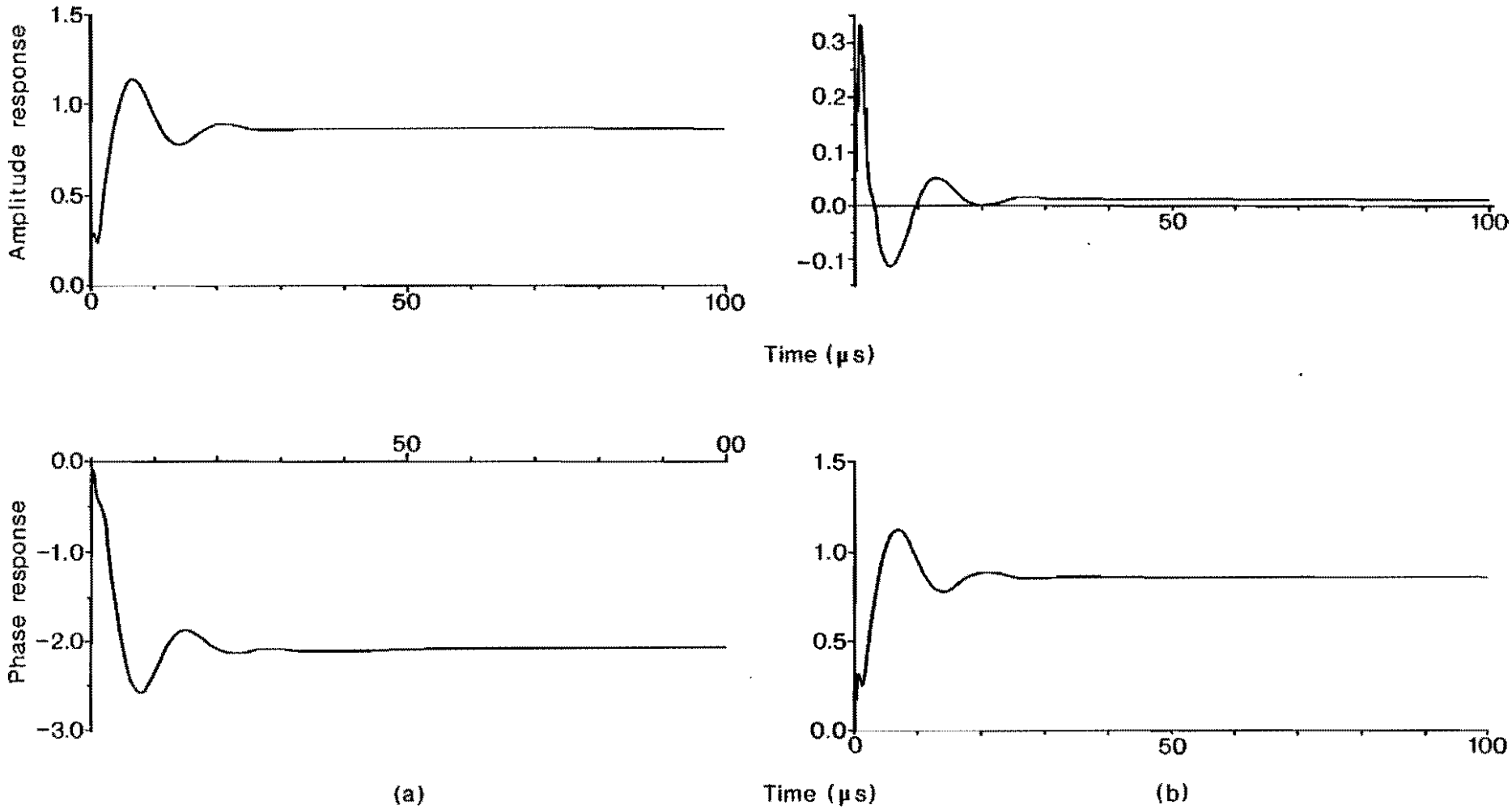
Amplitude response
1.5
1.0
0.5
0.0
0
50
100
0.3
0.2
0.1
0.0
-0.1
50
100
Time (μs)
50
00
0.0
-1.0
-2.0
-3.0
Phase response
1.5
1.0
0.5
0.0
0
50
100
Time (μs)
(a)
(b)

Fig. 7

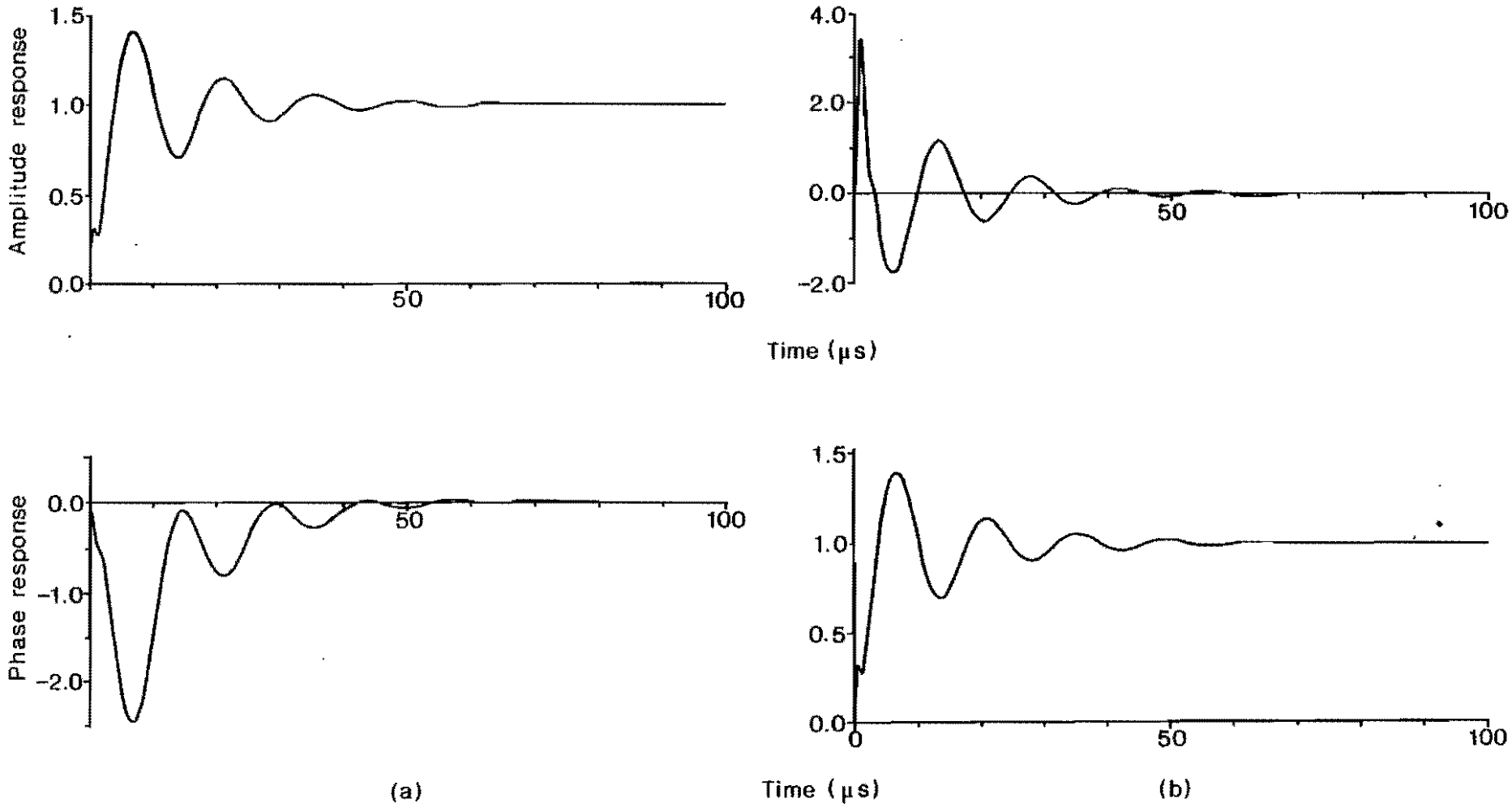
Amplitude response
1.5
1.0
0.5
0.0
50
100
4.0
2.0
0.0
-2.0
50
100
Time (μs)
Phase response
0.0
-1.0
-2.0
50
100
1.5
1.0
0.5
0.0
0
50
100
Time (μs)
(a)
(b)

Fig. 8

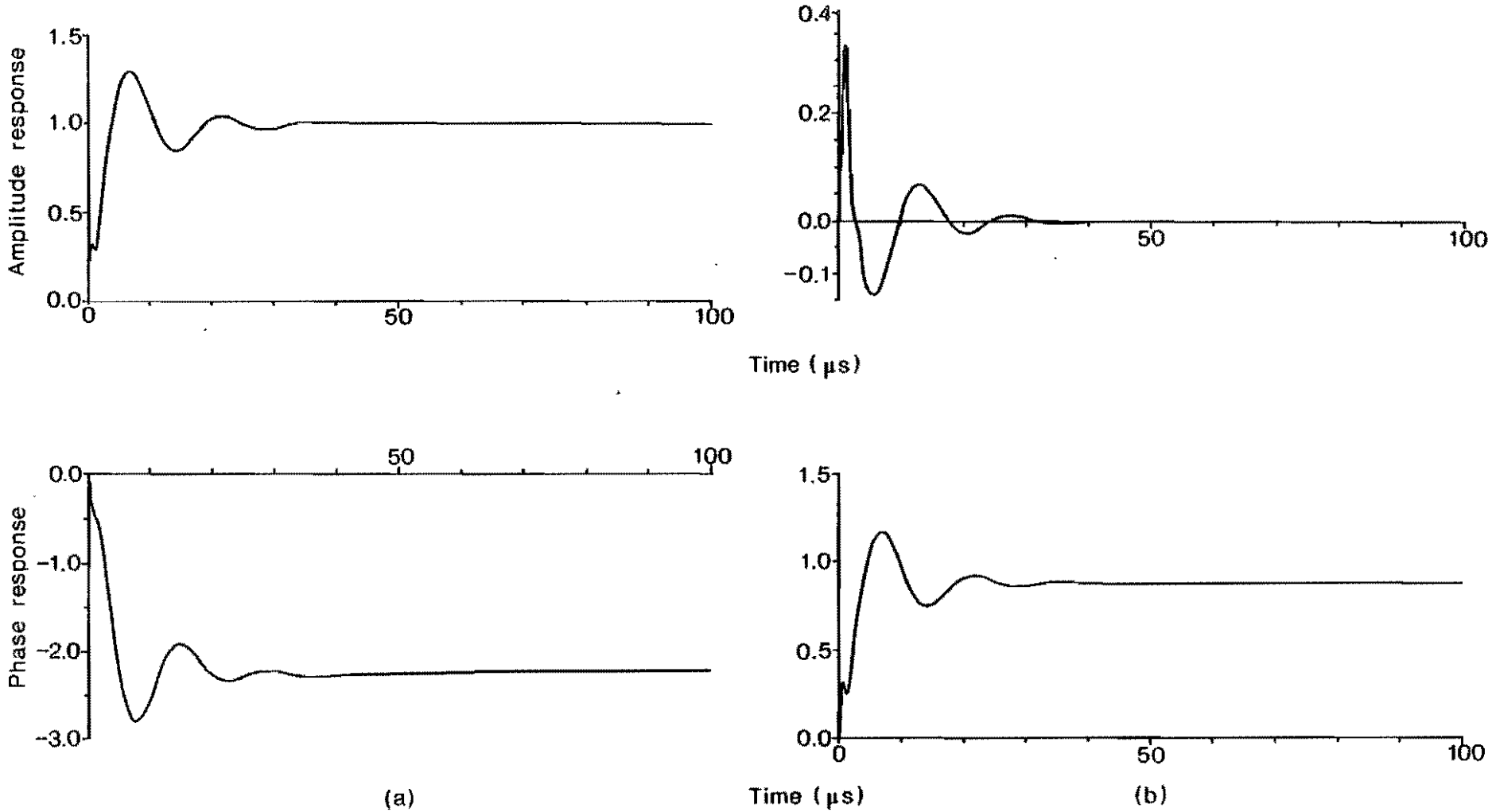
Amplitude response
1.5
1.0
0.5
0.0
0
50
100
0.4
0.2
0.0
-0.1
50
100
Time (μs)
50
100
0.0
-1.0
-2.0
-3.0
Phase response
(a)
1.5
1.0
0.5
0.0
0
50
100
Time (μs)
(b)

Fig.9

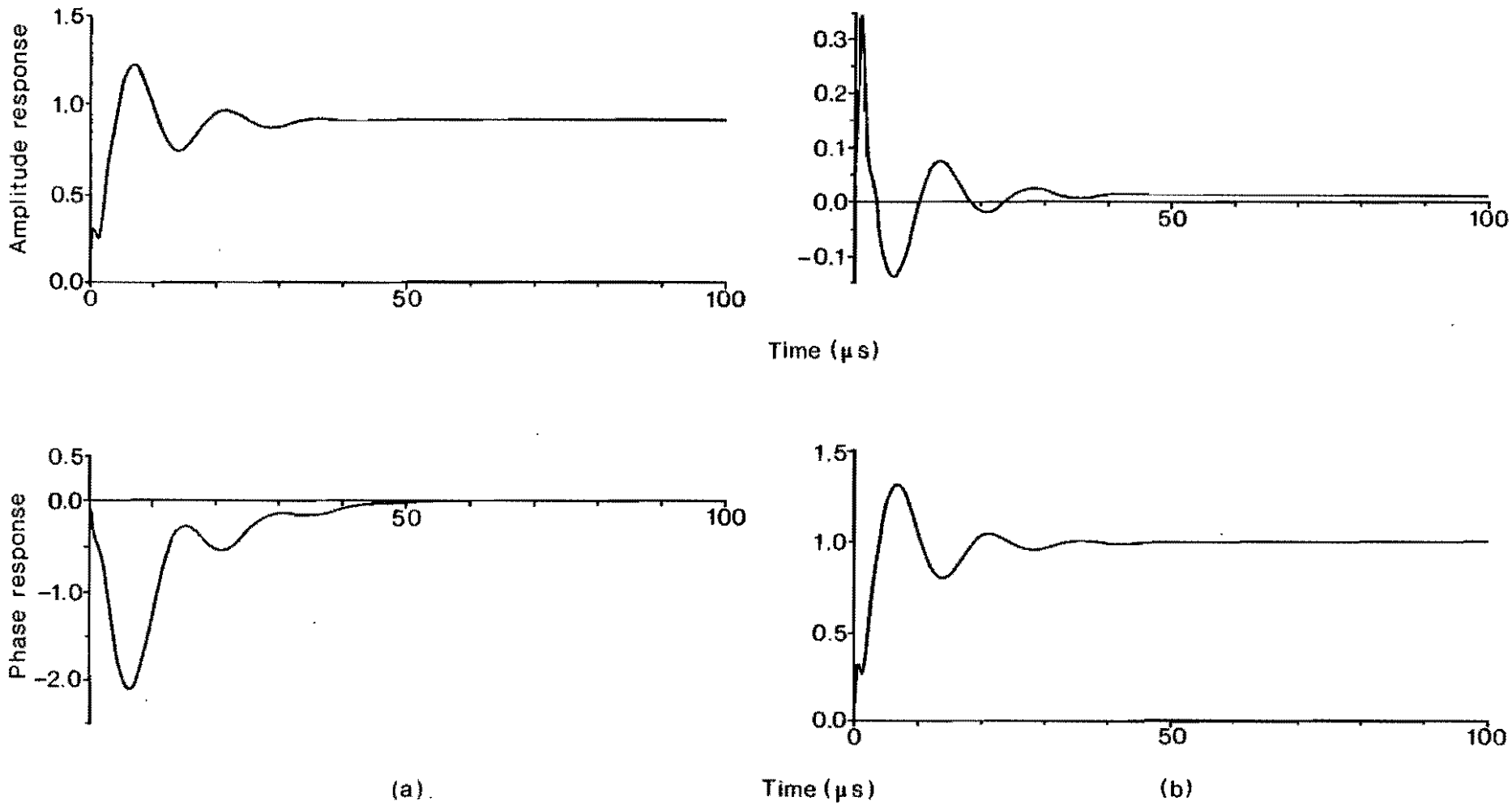
Amplitude response
1.5
1.0
0.5
0.0
0
50
100
0.3
0.2
0.1
0.0
-0.1
50
100
Time (μs)
Phase response
0.5
0.0
-1.0
-2.0
50
100
(a)
1.5
1.0
0.5
0.0
0
50
100
Time (μs)
(b)

Fig.10

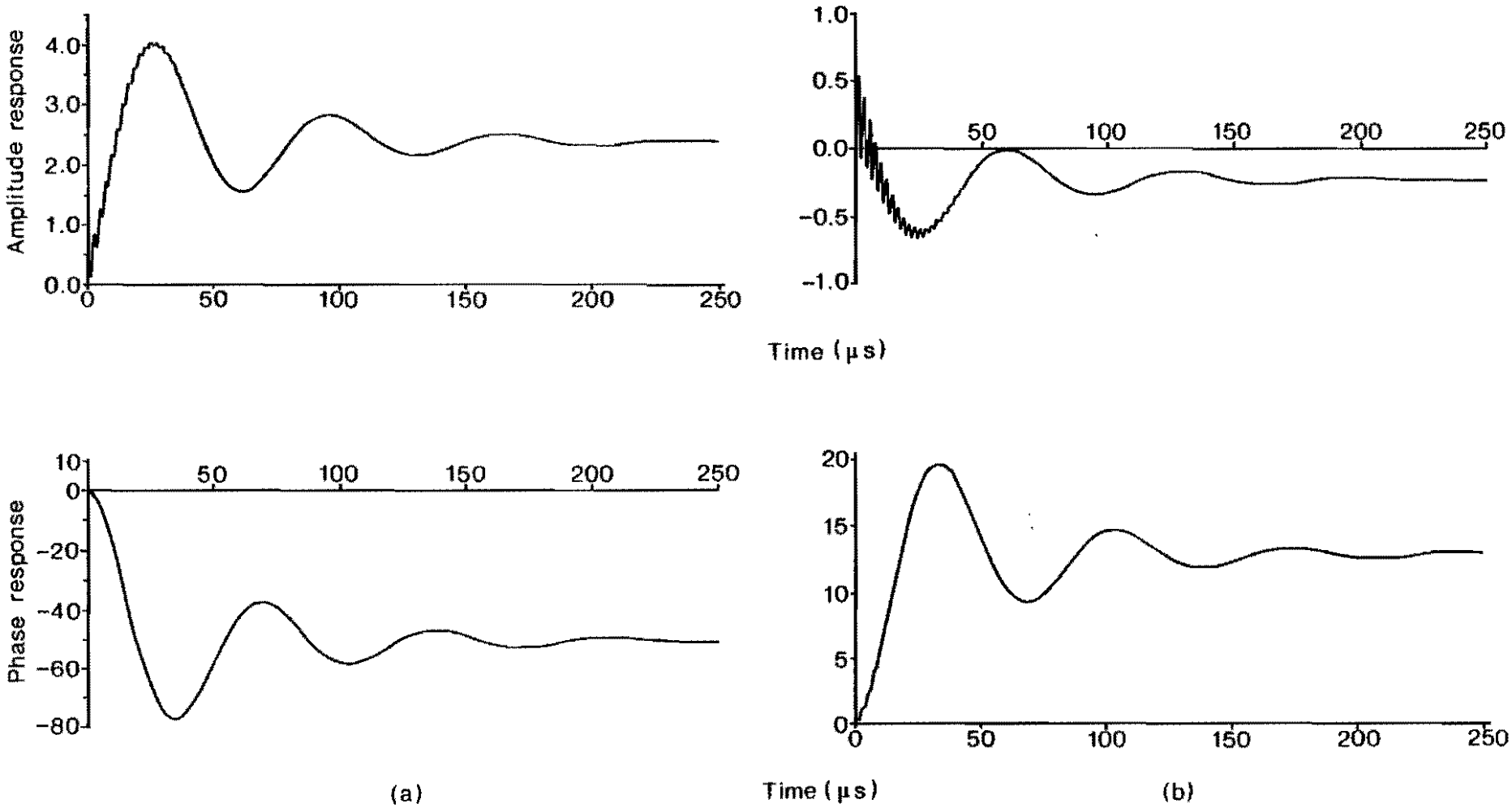
Amplitude response
4.0
3.0
2.0
1.0
0.0
0
50
100
150
200
250
1.0
0.5
0.0
-0.5
-1.0
50
100
150
200
250
Time (μs)
Phase response
10
0
-20
-40
-60
-80
50
100
150
200
250
20
15
10
5
0
0
50
100
150
200
250
Time (μs)

(a) (b)

Fig.11

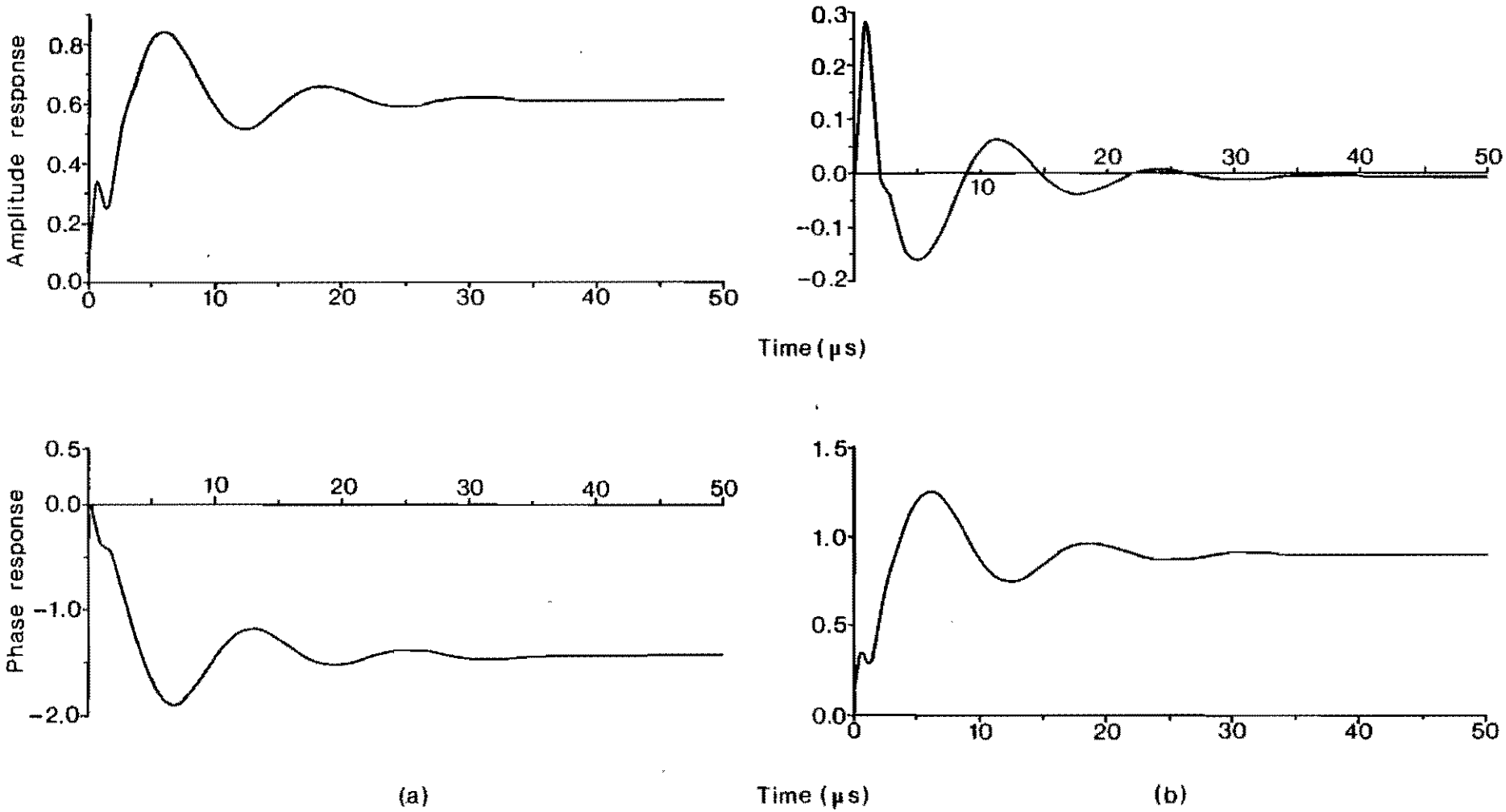
Amplitude response
0.8
0.6
0.4
0.2
0.0
0
10
20
30
40
50
0.3
0.2
0.1
0.0
-0.1
-0.2
10
20
30
40
50
Time (μs)
Phase response
0.5
0.0
-1.0
-2.0
10
20
30
40
50
(a)
1.5
1.0
0.5
0.0
0
10
20
30
40
50
Time (μs)
(b)

Fig. 12

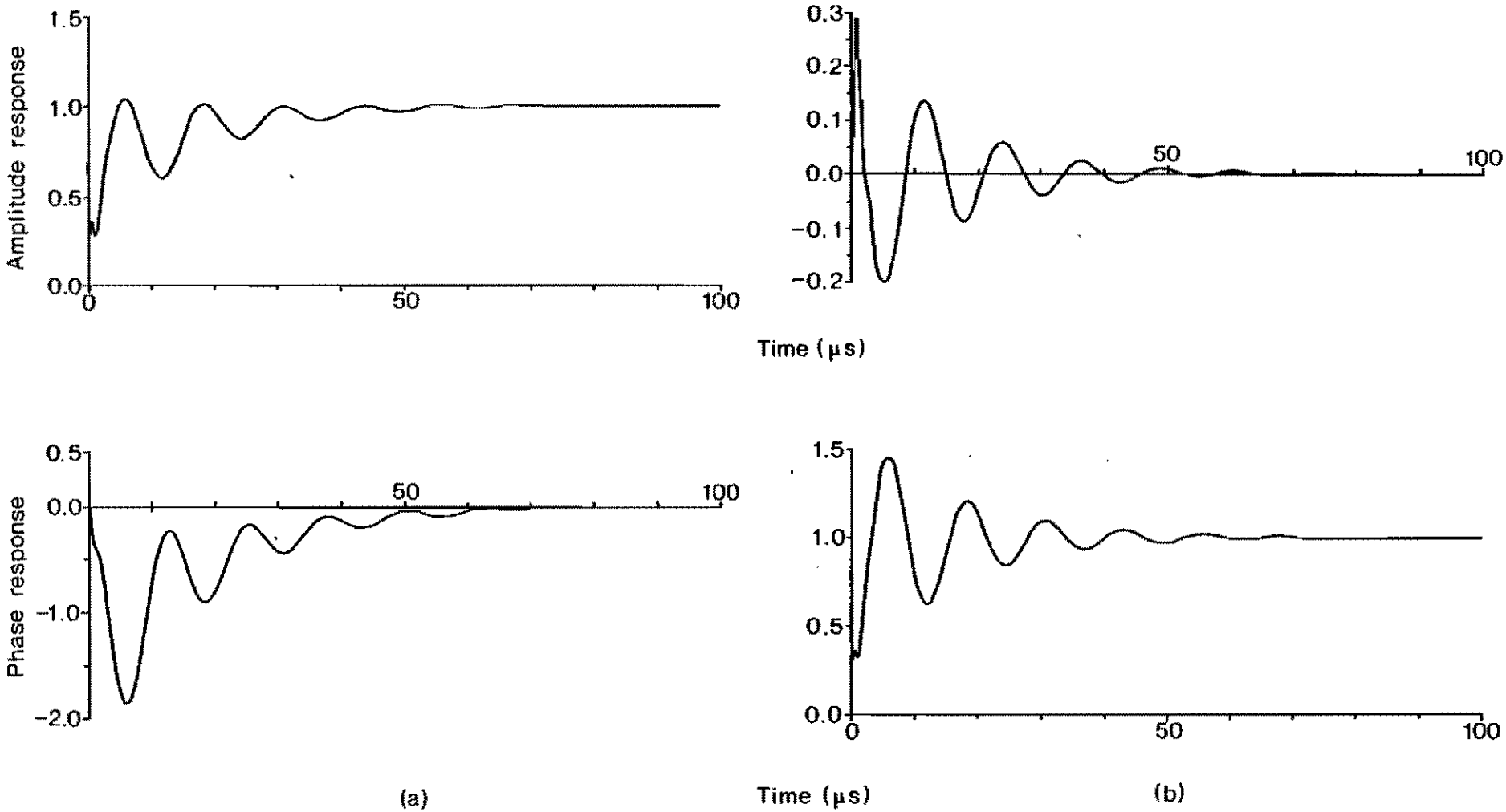
Amplitude response
1.5
1.0
0.5
0.0
0
50
100
0.3
0.2
0.1
0.0
-0.1
-0.2
50
100
Time (μs)
Phase response
0.5
0.0
-1.0
-2.0
50
100
(a)
1.5
1.0
0.5
0.0
0
50
100
Time (μs)
(b)

Fig.13

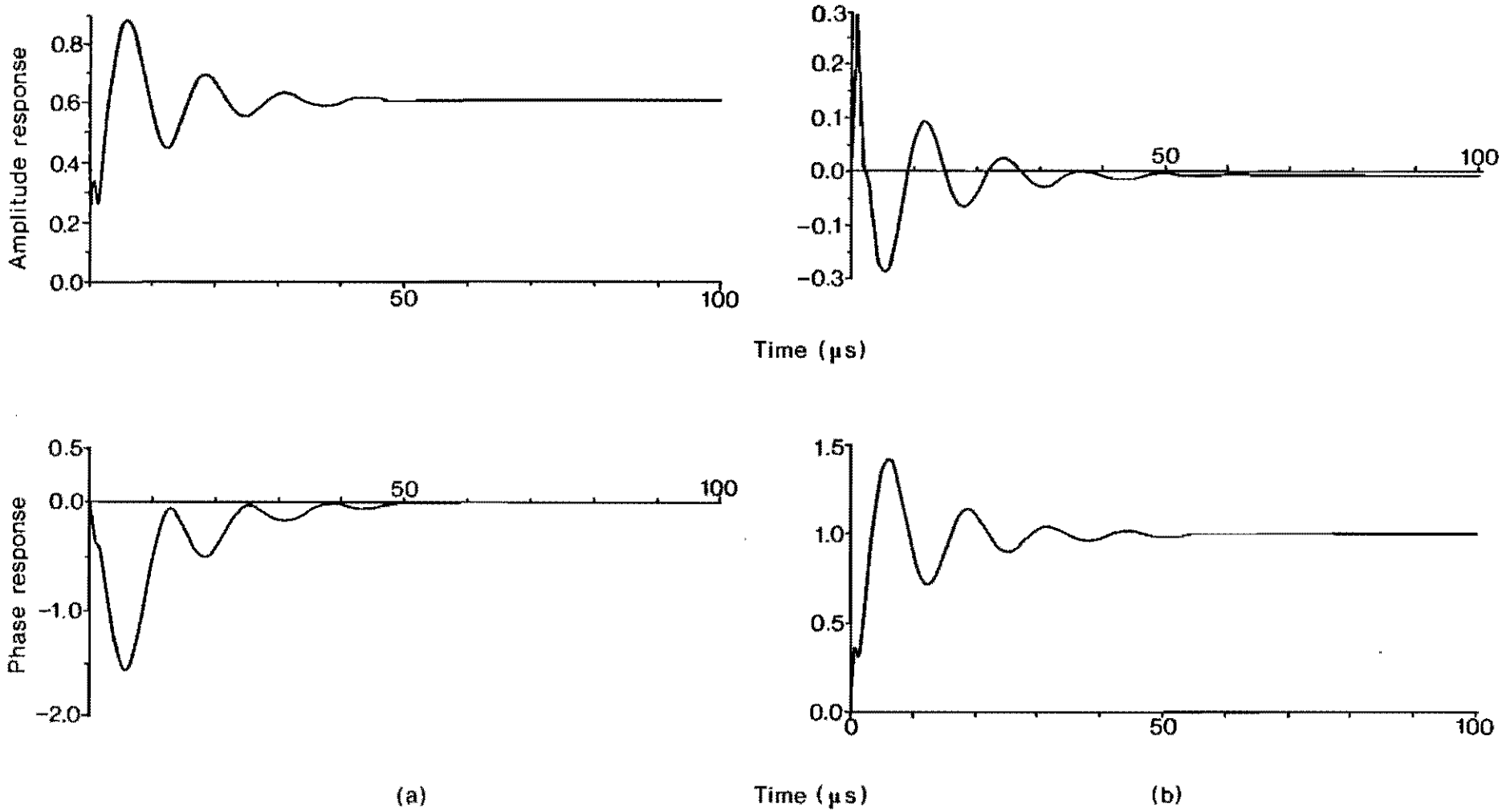
Amplitude response
0.8
0.6
0.4
0.2
0.0
50
100
0.3
0.2
0.1
0.0
-0.1
-0.3
50
100
Time (μs)
Phase response
0.5
0.0
-1.0
-2.0
50
100
1.5
1.0
0.5
0.0
0
50
100
(a)
Time (μs)
(b)

Fig.14

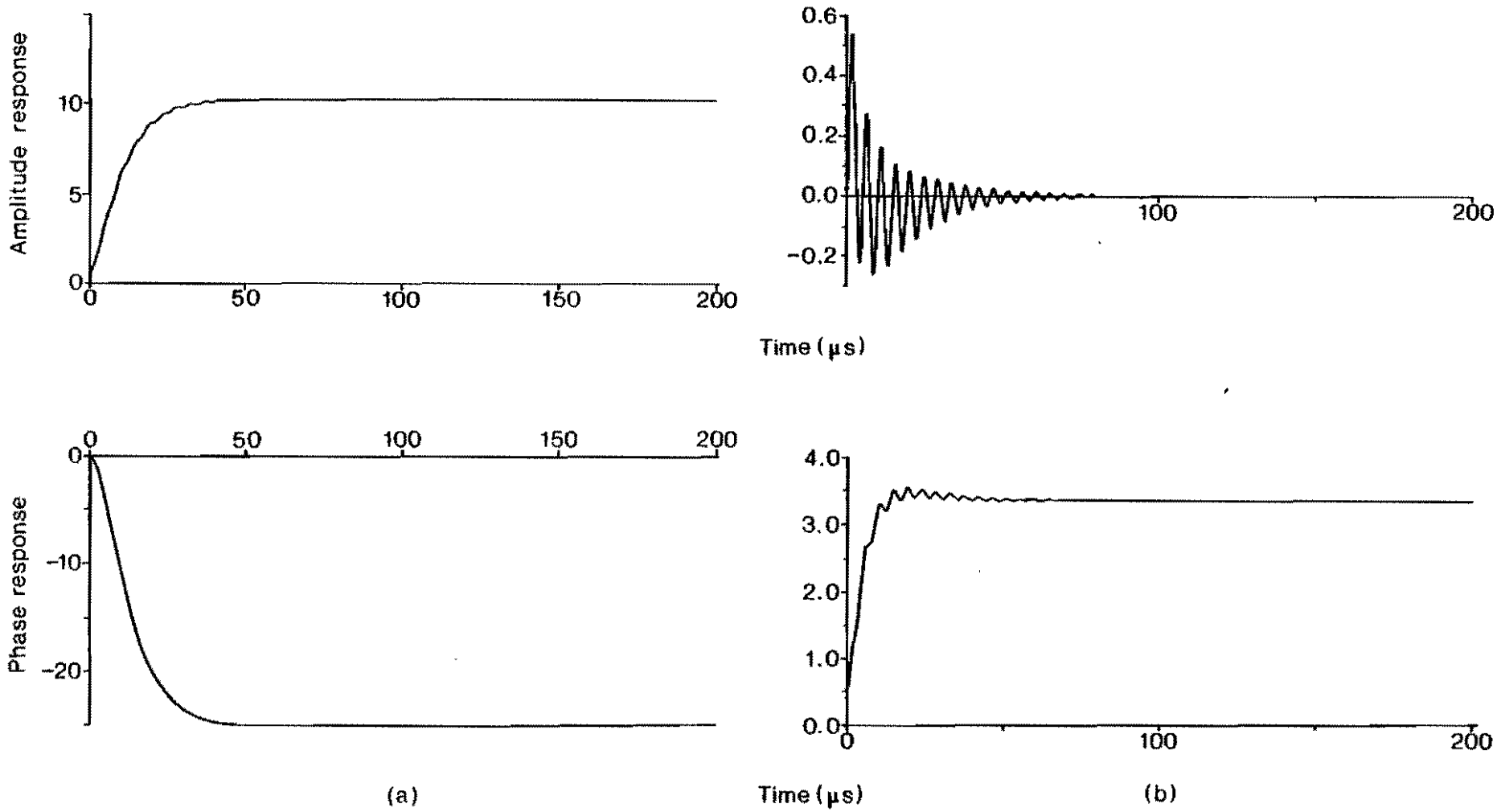
Amplitude response
10
5
0
0
50
100
150
200
Phase response
0
-10
-20
0
50
100
150
200
(a)
0.6
0.4
0.2
0.0
-0.2
100
200
Time (μs)
4.0
3.0
2.0
1.0
0.0
0
100
200
Time (μs)
(b)

Fig.15

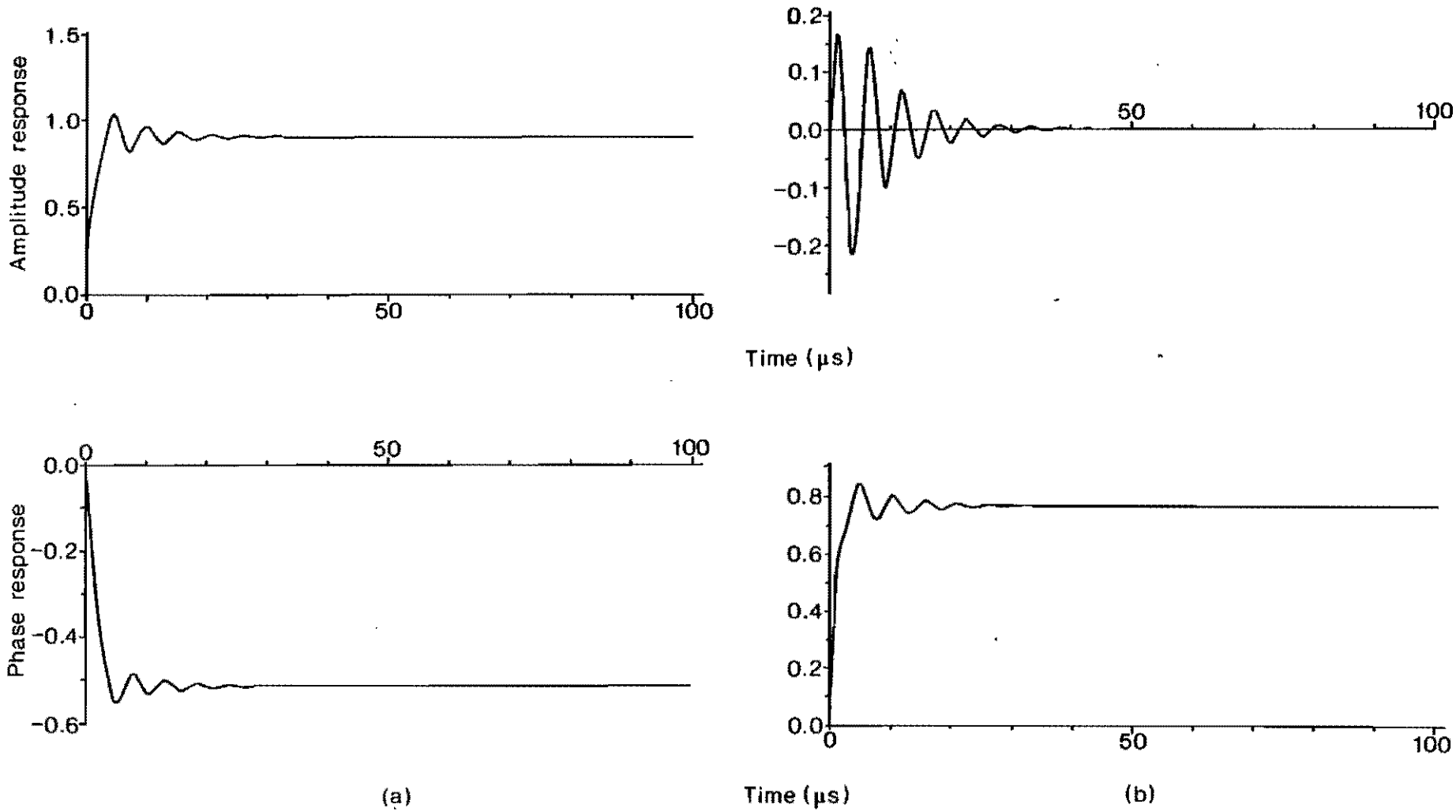
Amplitude response
1.5
1.0
0.5
0.0
0
50
100
0.2
0.1
0.0
−0.1
−0.2
50
100
Time (μs)
Phase response
0.0
−0.2
−0.4
−0.6
0
50
100
0.8
0.6
0.4
0.2
0.0
0
50
100
Time (μs)
(a)
(b)

Fig.16

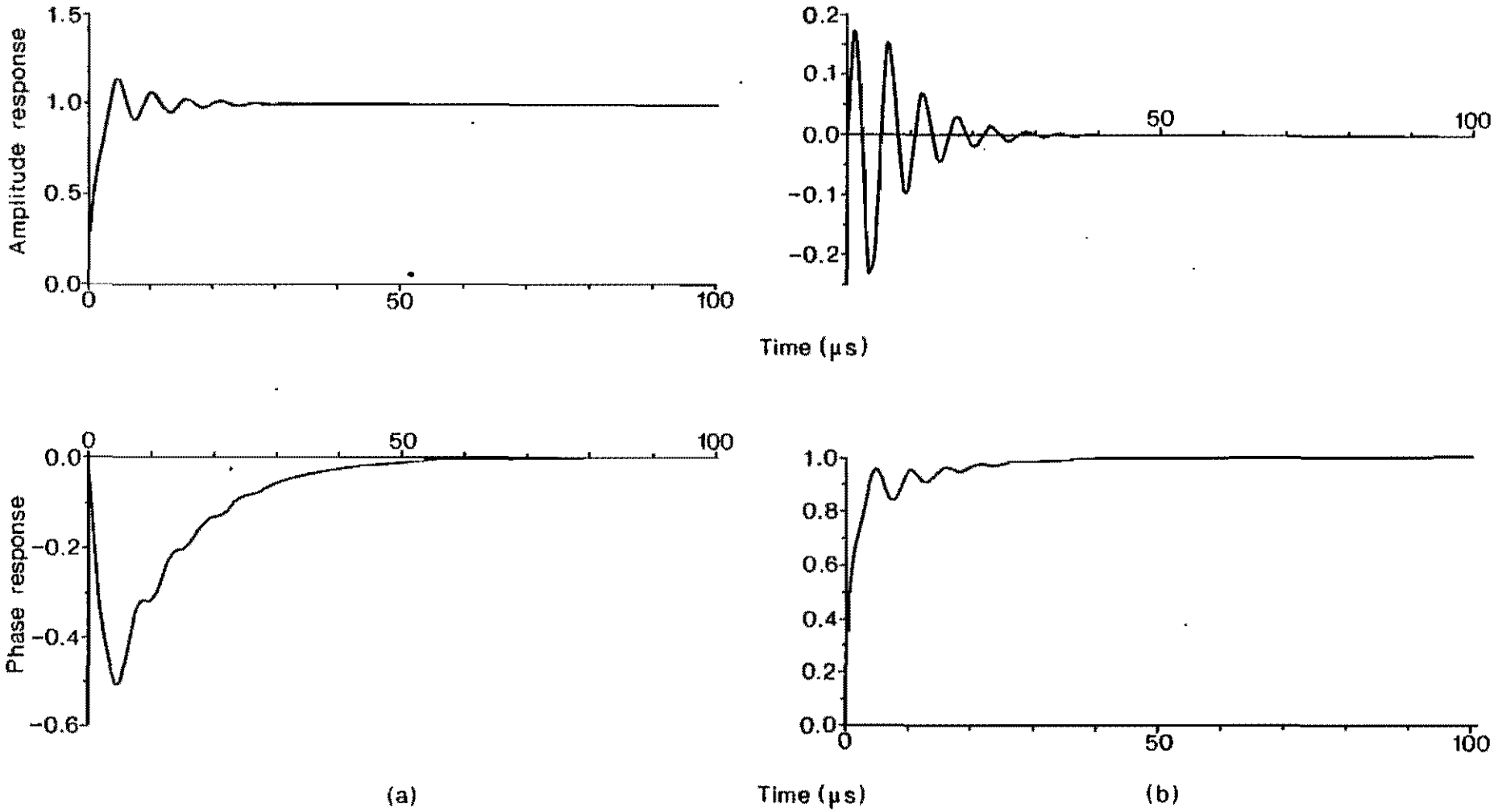
Amplitude response
1.5
1.0
0.5
0.0
0
50
100
0.2
0.1
0.0
-0.1
-0.2
50
100
Time (μs)
Phase response
0
50
100
0.0
-0.2
-0.4
-0.6
1.0
0.8
0.6
0.4
0.2
0.0
0
50
100
Time (μs)

(a) (b)

Fig.17

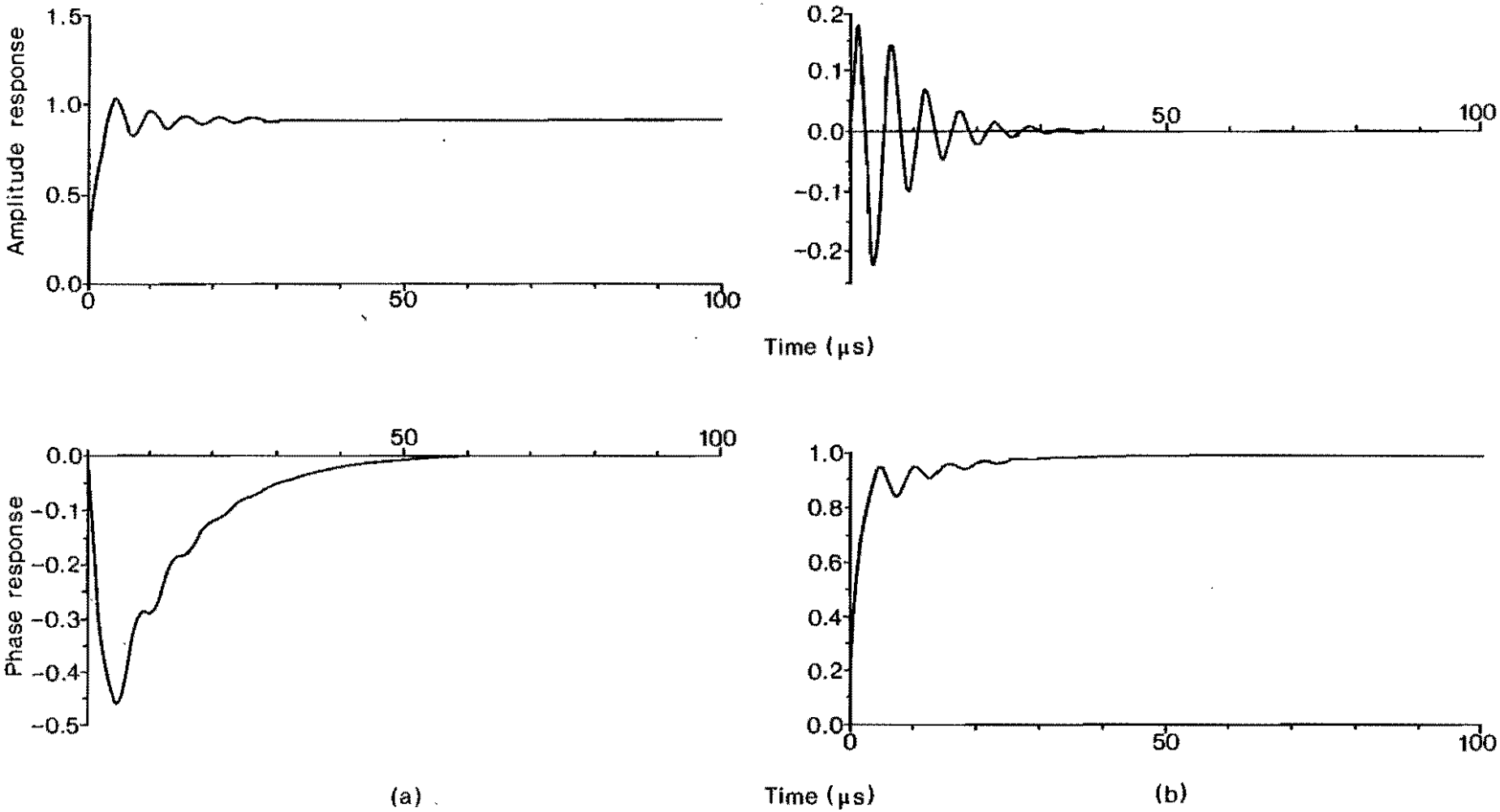
Amplitude response
1.5
1.0
0.5
0.0
0
50
100
0.2
0.1
0.0
-0.1
-0.2
50
100
Time (μs)
50
100
Phase response
0.0
-0.1
-0.2
-0.3
-0.4
-0.5
1.0
0.8
0.6
0.4
0.2
0.0
0
50
100
Time (μs)
(a)
(b)

Fig.18